

Topological chiral magnonic edge mode in a magnonic crystal

Ryuichi Shindou, Ryo Matsumoto, and Shuichi Murakami

Department of Physics, Tokyo Institute of Technology, 2-12-1 Ookayama, Meguro-ku, Tokyo, Japan

(Dated: March 2, 2013)

Topological phases have been explored in various fields in physics such as spintronics, photonics, liquid helium, correlated electron system and cold-atomic system. This leads to the recent foundation of emerging materials such as topological band insulators, topological photonic crystals and topological superconductors/superfluid. Here, we propose topological magnonic crystal which provides protected chiral edge modes for magnetostatic spin waves. Based on a generic linearized Landau-Lifshitz equation, we show that a magnonic crystal with the dipolar interaction usually acquires spin wave band with non-zero Chern integer. We argue that such magnonic systems are accompanied by the same integer numbers of chiral magnonic edge modes, along which the spin wave can propagate in a unidirectional manner without being backward scattered. Being a robust ‘one-way spin-wave guide’, the proposed chiral magnonic edge mode makes it possible the magnonic Fabry-Perot type interferometer, which can be utilized as the spin-wave logic gate.

Topological phases in condensed matters have been attracting much attention because of their fascinating physical properties. Discoveries of topological band insulators^{1–7} open up emerging research paradigm on spin-orbit interaction physics. Relativistic spin-orbit interaction in the topological band insulator endows its Bloch electron bands with non-trivial global structures, which lead to novel surface metallic states⁵ and topological magnetoelectric effect.⁸ Superconductor analogues of topological insulators have exotic edge modes⁹ or bound states,¹⁰ which are composed only of ‘real-valued’ fermion field dubbed as Majorana fermion. Some aspects of these bound states are experimentally confirmed,^{11,12} fostering much prospect of the realization of quantum computers.¹³ Photonics analogue of topological phase with chiral edge modes are proposed theoretically^{14,15} and are subsequently designed in actual photonics crystals.¹⁶ Unidirectional propagations of electromagnetic wave along these chiral edge modes were experimentally observed, which provides these metamaterials with unique photonic functionality.

Here, we theoretically propose a magnonics analogue of topological phases, which has topologically-protected chiral edge mode for spin waves. Spin wave is a collective propagation of precessional motions of magnetic moments in magnets. Depending on its wavelength, spin waves are classified into two categories. One is exchange spin-wave with the shorter wavelength, whose motion is driven by the quantum-mechanical exchange interactions (‘exchange-dominated’ region). The other is magnetostatic spin wave with the longer wavelength,^{17,18} whose propagation is caused by the long-range dipolar interaction (‘dipolar’ region). Magnonics research investigates how these spin waves propagate in the sub-micrometer length scale and sub-nanosecond time scale.^{19–25} Like in other solid-state technologies such as photonics, phononics and plasmonics, the main application direction is to explore ability of the spin wave to carry and process information. Especially, the propagation of spin waves

in periodically modulated magnetic materials dubbed as magnonic crystals^{21–23,26,27} are of one of its central concern. Owing to the periodic structuring, the spin wave spectrum in magnonic crystal acquires allowed frequency bands of spin wave states and forbidden-frequency bands (band gap).

We introduce a topological Chern number in these spin-wave bands with a band gap. Based on a simple magnonic crystal with wide varieties of material parameters, we predict that the first Chern number for the lowest spin-wave band usually takes non-zero integer values, when the wavelength is in the dipolar region. The relevant length scale turns out to be from sub- μm to hundreds of μm , well within the range of nanosize fabrication. The nonzero Chern integer in magnonic crystals results in the same integer numbers of topological chiral edge modes, along which the spin wave can propagate in a unidirectional way. Thanks to the topological protection, this propagation is generically free from any static backward scatterings. The unidirectional motion can be experimentally measurable especially in yttrium iron garnet (YIG), where the coherence length of magnons is on the order of centimeters.²⁰ We argue that these edge modes can be easily channelized, twisted, split and manipulated, which enables to construct novel magnonic devices such as spin-wave logic gate.

Chern number in boson systems

To introduce topological Chern number for the magnetostatic spin wave, let us consider a general quadratic Bogoliubov-de Gennes (BdG) Hamiltonian for boson fields in the two-dimensional momentum space (\mathbf{k} -space);

$$\mathcal{H} = \frac{1}{2} \sum_{\mathbf{k}} \begin{bmatrix} \beta_{\mathbf{k}}^{\dagger} & \beta_{-\mathbf{k}} \end{bmatrix} \cdot \mathbf{H}_{\mathbf{k}} \cdot \begin{bmatrix} \beta_{\mathbf{k}} \\ \beta_{-\mathbf{k}}^{\dagger} \end{bmatrix}. \quad (1)$$

with $\beta_{\mathbf{k}}^{\dagger} \equiv [\beta_{1,\mathbf{k}}, \dots, \beta_{N,\mathbf{k}}]$. N denotes the number of bosonic bands, and the $2N$ by $2N$ Hermite matrix $\mathbf{H}_{\mathbf{k}}$ is composed of the N by N normal parts (particle-hole

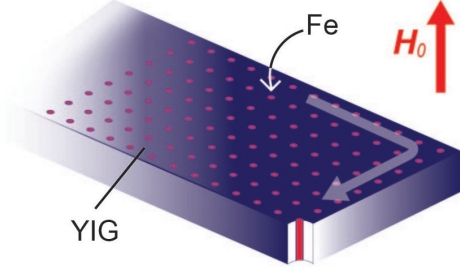


FIG. 1: **Magnonic crystal with chiral edge modes.** Periodic array of holes is introduced into YIG, forming a square lattice. Iron (Fe) is filled inside every hole.

channel) and N by N anomalous parts (particle-particle channel).

This bosonic BdG Hamiltonian is diagonalized in terms of a para-unitary matrix $\mathbf{T}_{\mathbf{k}}$ instead of a unitary matrix,²⁸

$$\mathbf{T}_{\mathbf{k}}^\dagger \mathbf{H}_{\mathbf{k}} \mathbf{T}_{\mathbf{k}} = \begin{bmatrix} \mathbf{E}_{\mathbf{k}} & \\ & \mathbf{E}_{-\mathbf{k}} \end{bmatrix}, \quad (2)$$

with $[\gamma_{\mathbf{k}}^\dagger, \gamma_{-\mathbf{k}}] \mathbf{T}_{\mathbf{k}}^\dagger = [\beta_{\mathbf{k}}^\dagger, \beta_{-\mathbf{k}}]$, and $\mathbf{E}_{\mathbf{k}}$ is a diagonal matrix. From the commutation relation for the γ -field, the orthogonality and completeness of the new basis are derived as

$$\mathbf{T}_{\mathbf{k}}^\dagger \sigma_3 \mathbf{T}_{\mathbf{k}} = \sigma_3, \quad \mathbf{T}_{\mathbf{k}} \sigma_3 \mathbf{T}_{\mathbf{k}}^\dagger = \sigma_3 \quad (3)$$

respectively, where the diagonal matrix σ_3 takes ± 1 in the particle/hole space, i.e. $[\sigma_3]_{jm} = \delta_{jm} \sigma_j$ with $\sigma_j = +1$ for $j = 1, \dots, N$ and $\sigma_j = -1$ for $j = N+1, \dots, 2N$. In terms of the para-unitary matrix, the field strength (Berry's curvature) B_j and the gauge connection (gauge field) $(A_{j,x}, A_{j,y})$ are introduced in the momentum space for j -th magnonic band as;

$$B_j \equiv \partial_{k_x} A_{j,y} - \partial_{k_y} A_{j,x}, \quad (4)$$

$$A_{j,\nu} \equiv i \text{Tr}[\mathbf{\Gamma}_j \sigma_3 \mathbf{T}_{\mathbf{k}}^\dagger \sigma_3 (\partial_{k_\nu} \mathbf{T}_{\mathbf{k}})], \quad (5)$$

respectively with $j = 1, \dots, 2N$. $\mathbf{\Gamma}_j$ is a $2N$ by $2N$ diagonal matrix taking $+1$ for the j -th diagonal component and zero otherwise. The Chern number (the first Chern number) associated with the j -th band is given by the momentum integral of the respective Berry's curvature over the two-dimensional first Brillouin zone (BZ),

$$C_j = \frac{1}{2\pi} \int_{\text{BZ}} d^2 \mathbf{k} B_j. \quad (6)$$

This quantity can be shown to be an integer $C_j = n$ (see Supplementary Information for details), which corresponds to a number of topological chiral edge modes. Note that, due to the commutation relation of the boson fields, the Chern integer defined in equations (4,5,6) generally takes a form different from those

Chern integers previously defined in electronic²⁹ and photonic^{14,15,30} systems. In the following, we show that a two-dimensional magnonic crystal (MC) with the dipolar interaction usually supports spin-wave bands with non-zero Chern integers.

2-d magnonic crystals and dipolar interaction

The MC considered is a ferromagnetic system with its magnetization and exchange interaction modulated periodically in the 2-dimensional (x - y) direction. For simplicity, we assume that the system is translationally symmetric along the z -direction, whereas the subsequent results are expected to be similar when the thickness of the system in the z -direction becomes finite. The system is composed of two kinds of ferromagnets; iron and YIG. The unit cell of the MC is an $a_x \times a_y$ rectangle, inside which iron is embedded into a circular region, while the remaining region is filled with YIG (Fig. 1). The uniform magnetic field H_0 is applied along the z direction, such that the static ferromagnetic moment M_s in both regions is fully polarized in the z direction. Propagation of the transverse moments (m_x, m_y) is described by a linearized Landau-Lifshitz equation^{26,27,31,32},

$$\begin{aligned} \frac{1}{|\gamma|\mu_0} \frac{dm_{\pm}}{dt} = & \pm 2iM_s (\nabla \cdot Q \nabla) m_{\pm} \mp 2im_{\pm} (\nabla \cdot Q \nabla) M_s \\ & \mp iH_0 m_{\pm} \pm ih_{\pm} M_s \end{aligned} \quad (7)$$

with $\nabla \equiv (\partial_x, \partial_y)$, $m_{\pm} = m_x \pm im_y$ and $h_{\pm} = h_x \pm ih_y$. (h_x, h_y) stands for the transverse component of long-ranged magnetic dipolar field \mathbf{h} , which is related to the ferromagnetic moment $\mathbf{m} \equiv (m_x, m_y, M_s)$ via the Maxwell equation, i.e. $\nabla \times \mathbf{h} = c^{-1} \partial_t \mathbf{e}_z$ and $\nabla \cdot (\mathbf{h} + \mathbf{m}) = 0$. The former two terms in the right hand side of equation (7) comes from short-ranged exchange interaction, where Q denotes the square of the exchange interaction length. M_s and Q take the values of iron inside the circular region, while taking the values of YIG otherwise. The filling fraction of the circular region with respect to the total area of the unit cell is parameterized by f . We restrict ourselves to the wavelength much longer than atomic lattice constants of YIG and iron, so that the use of this Landau-Lifshitz equation is justified. Since the velocities of relevant spin-wave modes are much smaller than the speed of light, we can further employ the magneto-static approximation, replacing the Maxwell equations by $\nabla \times \mathbf{h} = 0$ and $\nabla \cdot (\mathbf{h} + \mathbf{m}) = 0$;

$$h_{\nu} = -\partial_{\nu} \Psi, \quad \Delta \Psi = \partial_x m_x + \partial_y m_y, \quad (8)$$

with $\nu = x, y$. This in combination with equation (7) gives a closed equation of motion (EOM) for the transverse moments. In terms of normalized transverse fields;

$$\beta(\mathbf{r}) \equiv \frac{m_+(\mathbf{r})}{\sqrt{2M_s(\mathbf{r})}}, \quad \beta^\dagger(\mathbf{r}) \equiv \frac{m_-(\mathbf{r})}{\sqrt{2M_s(\mathbf{r})}}. \quad (9)$$

with a proper commutator $[\beta(\mathbf{r}), \beta^\dagger(\mathbf{r}')] = \delta(\mathbf{r} - \mathbf{r}')$, the coupled EOM reduces to an equivalent generalized eigenvalue problem with a Hermitian matrix $\mathbf{H}_{\mathbf{k}}$ (see Methods

for details);

$$i \frac{d}{dt} \begin{bmatrix} \beta_{\mathbf{k}} \\ \beta_{-\mathbf{k}}^\dagger \end{bmatrix} = \sigma_3 \mathbf{H}_{\mathbf{k}} \begin{bmatrix} \beta_{\mathbf{k}} \\ \beta_{-\mathbf{k}}^\dagger \end{bmatrix}, \quad (10)$$

where $\beta_{\mathbf{k}}^\dagger$ denotes a vector composed of the Fourier series of $\beta^\dagger(\mathbf{r})$ with respect to the reciprocal vector \mathbf{G} ; $\beta_{\mathbf{k}}^\dagger \equiv [\dots, \beta_{\mathbf{k}}^\dagger(\mathbf{G}), \dots]$ and $\beta(\mathbf{r}) = \sum_{\mathbf{k}, \mathbf{G}} \beta_{\mathbf{k}}(\mathbf{G}) e^{-i(\mathbf{k} + \mathbf{G})\mathbf{r}}$. The EOM is diagonalized in terms of a para-unitary matrix $\mathbf{T}_{\mathbf{k}}$ introduced in equation (2) as

$$i \frac{d}{dt} \begin{bmatrix} \gamma_{\mathbf{k}} \\ \gamma_{-\mathbf{k}}^\dagger \end{bmatrix} = \begin{bmatrix} \mathbf{E}_{\mathbf{k}} & \\ & -\mathbf{E}_{-\mathbf{k}} \end{bmatrix} \begin{bmatrix} \gamma_{\mathbf{k}} \\ \gamma_{-\mathbf{k}}^\dagger \end{bmatrix}.$$

$[\mathbf{E}_{\mathbf{k}}]_j$ gives the dispersion of the j -th magnonic band ($j = 1, \dots$), while $[\mathbf{T}_{\mathbf{k}}]_{a,j}$ ($a = \dots, \mathbf{G}, \dots$) stands for the periodic part of the j -th magnonic Bloch wavefunction. Correspondingly, the Chern integer is defined for each magnonic band via equations (6), (4) and (5).

The topological Chern integer thus calculated always reduces to zero, whenever the system considered is either time-reversal symmetric; $\mathbf{H}_{-\mathbf{k}}^* = \mathbf{H}_{\mathbf{k}}$, or mirror-symmetric with the mirror plane being perpendicular to the xy plane, e.g. $\mathbf{H}_{(k_x, k_y)} = \mathbf{H}_{(k_x, -k_y)}$. Owing to the dipolar interaction, however, the anomalous part of $\mathbf{H}_{\mathbf{k}}$ acquires a complex-valued phase factor which depends on the momentum in the chiral way (see Methods for details). As a result, these two symmetries are generically absent in the 2- d MCs and the bosonic Chern integer can take a non-zero integer value.

This situation is quite analogous to what the relativistic spin-orbit interaction does in ferromagnetic metals^{33,34} and topological band insulators.^{1,2,4,5} Moreover, contrary to the relativistic spin-orbit interaction, the strength of the dipolar interaction is an experimentally tunable parameter in the MCs.²¹ Namely, the dimensional analysis on equation (7) indicates that, when the characteristic length scale of the MC (the unit cell size $\lambda \equiv \sqrt{a_x a_y}$) becomes larger than the typical exchange length \sqrt{Q} , the dipolar interaction prevails over the exchange interaction.

Chiral magnonic bands in MC

We found that the Chern integer of the lowest magnonic band, C_1 , is always quantized to be 2 for the longer λ , while the integer reduces to zero for the shorter λ (Fig. 2a). The respective quantization is protected by a finite direct band gap between the lowest band and the second lowest band (Fig. 2b). In the intermediate regime of λ , these two bands get closer to each other. With the four-fold rotational symmetry ($r \equiv a_y/a_x = 1$), the gap closes at the two X -points at a critical value of λ ($\sim 0.28\mu\text{m}$), where the two bands form gapless Dirac spectra (Fig. 2c). Without the four-fold symmetry ($r \neq 1$), the band touching at one of the two X points and that of the other occur at different values of λ . These band-touchings are $P_1(\pi, 0, \lambda_{c,1})$ and $P_2(0, \pi, \lambda_{c,2})$ in the

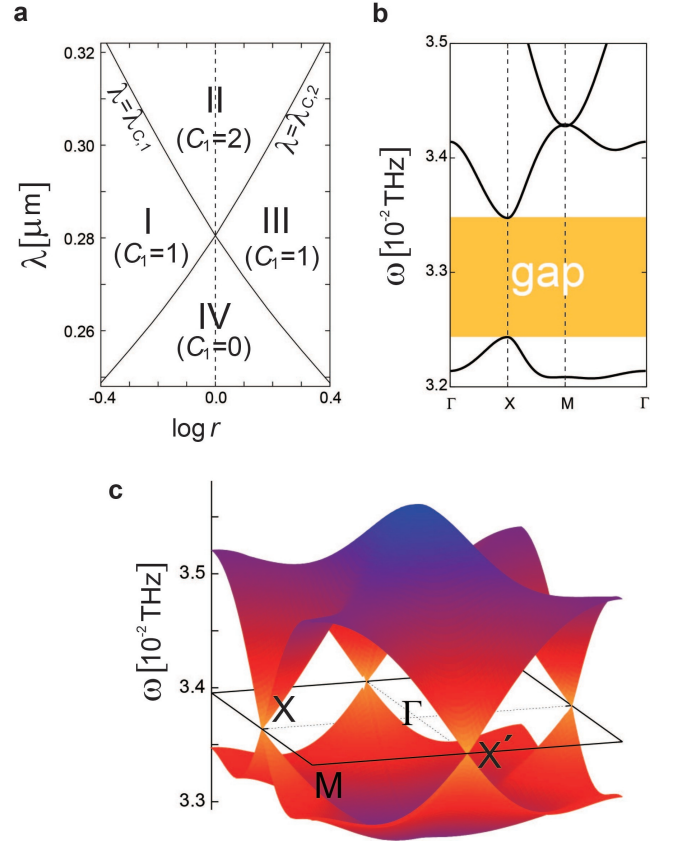


FIG. 2: **Chern-integer phase diagram for the lowest magnonic band and band dispersions of several lowest magnonic bands.** **a**, Chern-integer phase diagram for the lowest magnonic band as a function of the linear dimension of the unit cell size ($\lambda \equiv \sqrt{a_x a_y}$) and the aspect ratio of the unit cell ($r \equiv a_y/a_x$) with $f = \pi \times 10^{-2}$. The phases are characterized by the Chern integer of the lowest magnonic band, C_1 . **b**, Band dispersions of the lowest three magnonic bands with $r = 1$, $\lambda = 0.35\mu\text{m}$ and $f = \pi \times 10^{-2}$. A magnonic band gap appears between the first and the second lowest band, whose size is on the order of 10^{-3}THz . **c**, Band dispersions of the lowest and second lowest magnonic band at the critical point which intervenes the phase II ($C_1 = 2$) and the phase IV ($C_1 = 0$). Dirac cones with same chiralities are formed at the two inequivalent X points.

3-dimensional parameter space subtended by two crystal momenta k_x and k_y and the unit cell size λ (Fig. 3).

As in the fermionic case,^{35,36} a band-touching point in the 3- d parameter space generally plays a role of the dual magnetic monopole (charge). The dual magnetic field considered is a vector field defined in the parameter space (k_x, k_y, λ) , generalized from equation (4) as the ‘rotation’ of three-component gauge field $\mathbf{A}_j \equiv (A_{j,x}, A_{j,y}, A_{j,\lambda})$;

$$\mathbf{B}_j \equiv \nabla \times \mathbf{A}_j, \quad (11)$$

with $\nabla \equiv (\partial_{k_x}, \partial_{k_y}, \partial_{\lambda})$. Here the third component of the gauge field $A_{j,\lambda}$ is newly introduced in the same way

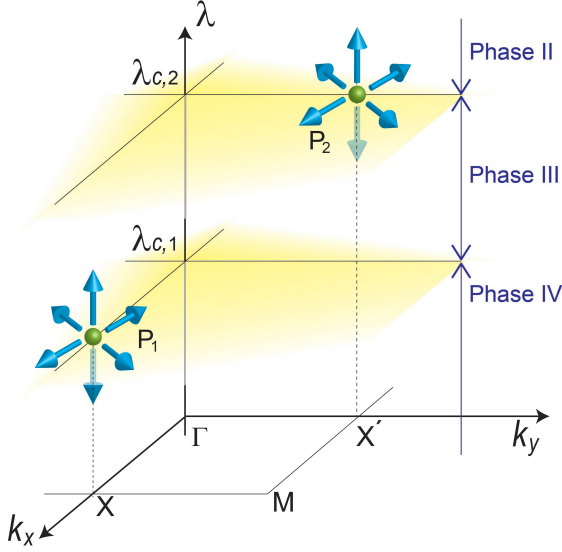


FIG. 3: **Schematic configuration of dual magnetic monopoles in the 3-dimensional parameter space subtended by the crystal momenta (k_x, k_y) and the linear dimension of the unit cell size $(\lambda \equiv \sqrt{a_x a_y})$ for $r \equiv a_y/a_x > 1$.** Small green spheres denote the magnetic monopoles, which emit the dual magnetic field (blue arrows). We only show the first quadrant of the Brillouin zone. Three phases found in Fig. 2a with $r > 1$ are separated by the $\lambda = \lambda_{c,2}$ plane and the $\lambda = \lambda_{c,1}$ plane. A magnetic monopole located on each plane means that the ‘phase transition’ is accompanied by the change of the Chern integer.

as previously done in (5);

$$A_{j,\lambda} \equiv i\text{Tr}[\mathbf{\Gamma}_j \sigma_3 T_{\mathbf{k}}^\dagger \sigma_3 (\partial_\lambda T_{\mathbf{k}})]. \quad (12)$$

j specifies either one of the two magnonic bands which form the band-touching. At the band-touching point, the dual magnetic field for the respective bands has a dual magnetic charge, whose strength is quantized to be 2π times integer (see Supplementary Information).

We found that dual magnetic charges for the lowest band at the band touching points at P_1 and P_2 are both $+2\pi$ (Fig. 3); $\nabla \cdot \mathbf{B}_1 = 2\pi\delta(\lambda - \lambda_{c,1})\delta(k_x - \pi)\delta(k_y) + 2\pi\delta(\lambda - \lambda_{c,2})\delta(k_x)\delta(k_y - \pi)$, where $\lambda_{c,1} < \lambda_{c,2}$ for $a_y > a_x$ ($r > 1$) and $\lambda_{c,1} > \lambda_{c,2}$ for $a_y < a_x$ ($r < 1$). The Gauss theorem suggests that, when the unit cell size λ is varied across one of these band-touching points ($\lambda_{c,1}$ or $\lambda_{c,2}$), the Chern integer for the lowest magnonic band changes by unity, e.g.

$$C_1|_{\lambda > \lambda_{c,1}} - C_1|_{\lambda_{c,1} > \lambda} = \frac{1}{2\pi} \int_{S_1} d\mathbf{n} \cdot \mathbf{B}_1 = 1,$$

where S_1 is a small sphere enclosing the magnetic charge at P_1 in the 3- d parameter space. This leads to the phase diagram in Fig. 2a, which describes the Chern integer of the lowest magnonic band as a function of the unit cell

size λ and the aspect ratio r . There are four phases, divided by the curves $\lambda = \lambda_{c,1}$ and $\lambda = \lambda_{c,2}$.

A dual magnetic charge is a quantized object, so that it can neither disappear by itself nor change gradually. Upon any small change of material parameters, two magnetic charges can only move around in the 3- d parameter space. Moreover, in the presence of the spatial inversion symmetry $\mathbf{H}_{\mathbf{k}} = \mathbf{H}_{-\mathbf{k}}$, their locations are always restricted at the X points. As a result, the global structure of the phase diagram depicted in Fig. 2a widely holds true for other combinations of material parameters. In fact, for $r = 1$ and $f = \pi \times 10^{-2}$, we found $\lambda_c = 0.370\mu\text{m}$ for iron (circular region) and YIG (host), and $\lambda_c = 0.372\mu\text{m}$ for cobalt (circular region) and YIG (host). When varying the filling fraction for iron (circular region) and YIG (host) with $r = 1$, we found $\lambda_c = 0.274\mu\text{m}$ for $f = 4\pi \times 10^{-2}$, and $\lambda_c = 0.348\mu\text{m}$ for $f = 9\pi \times 10^{-2}$. From these observations, we expect that, even if materials in the circular region is replaced simply by the vacuum, the MC systems with larger unit cell size still belongs to topological non-trivial phases, having nonzero Chern integers.

Chiral magnonic edge mode in MC

The chiral phases with non-zero Chern integers have chiral magnonic edge modes, which are localized at the boundary with the phase with zero Chern integer (phase IV) or the vacuum. These chiral modes carry spin wave in a unidirectional manner, whose dispersions go across the band gap between the lowest and the second lowest band. As an illustrative example, we consider a boundary (y axis) between the MC in phase III and MC in the phase IV, whose Chern integers for the lowest magnonic bands differ by unity (Fig. 4a). The existence of a chiral magnonic edge mode between these two is shown from a 2 by 2 Dirac Hamiltonian derived near their phase boundary ($\lambda = \lambda_{c,1}$). The Hamiltonian generally takes a following form (see Supplementary Information),

$$\mathcal{H}_{\text{eff}} = \omega_0 \tau_0 + \kappa(x) \tau_3 - ia \partial_x \tau_1 - ib \partial_y \tau_2. \quad (13)$$

τ_j denotes the Pauli matrices subtended by the two-fold degenerate eigenstates with their eigen-frequency ω_0 , which are formed by the lowest magnonic band and second lowest one at P_1 . a and b are constant material parameters which are positive-valued. The difference of the Chern integers (C_1) for the two phases is represented as a change of the sign of the Dirac mass term $\kappa(x)$; we hence suppose that positive $\kappa(x)$ for $x > 0$ is for the phase III and negative $\kappa(x)$ for $x < 0$ is for the phase IV (see Fig. 4a); $\lim_{x \rightarrow \pm\infty} \kappa(x) = \pm\kappa_\infty$. The Hamiltonian has a following eigenstate;^{37,38}

$$\psi_{\mathbf{k}}(\mathbf{r}) \propto e^{iky} e^{-\frac{1}{a} \int^x \kappa(x') dx'} \begin{bmatrix} 1 \\ i \end{bmatrix}.$$

which is localized at the boundary ($x = 0$). In terms of the surface crystal momentum k along the y axis, the

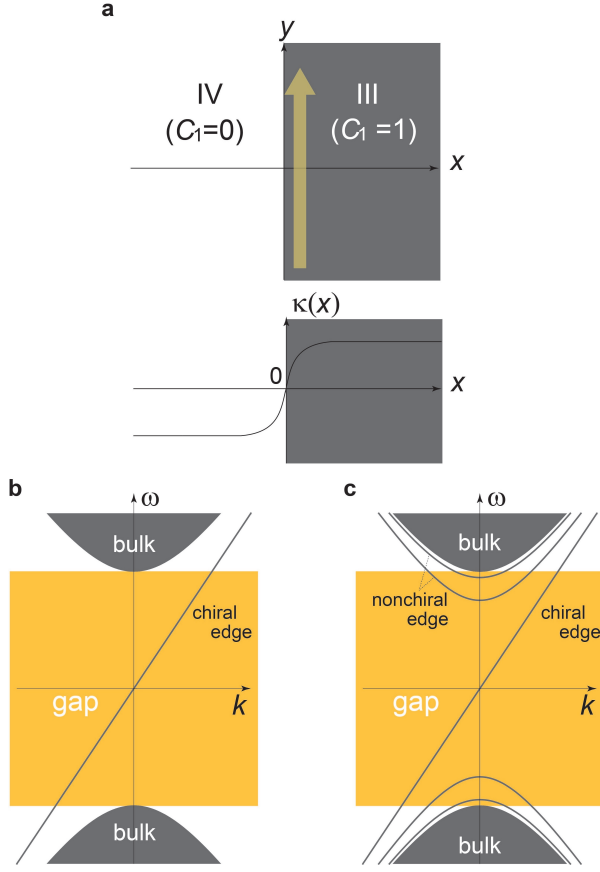


FIG. 4: **Chiral magnonic edge modes.** **a**, geometry of the system. **bc**, dispersions for Dirac Hamiltonian with the Pöschl-Teller potential¹⁵ $\kappa(x) = \kappa_\infty \tanh(x/d)$ for $\kappa_\infty d = 0.9a$ (**b**) and $\kappa_\infty d = 2.9a$ (**c**). The bulk magnonic bands ('bulk') have a gap, and one chiral edge state runs across the gap. In **c** there are some nonchiral edge states, whereas in **b** there is not. Nonetheless, the number of chiral edge modes is one, which is determined solely from the difference between the Chern integers for the two phases.

corresponding eigen-frequency is given by $E = \omega_0 + bk$. This connects the lowest magnonic band lying at $E \leq \omega_0 - \kappa_\infty$ and the second lowest band at $E \geq \omega_0 + \kappa_\infty$ (see Fig. 4b,c). The mode is chiral, since it propagates along the boundary in a unidirectional way, $v_k \equiv \partial_k E = b$. The argument so far can be generalized into other situations. The generalization suggests that the phase with $C_1 = 1$ at $r > 1$ (Phase III) or $r < 1$ (Phase I) has a chiral edge mode at its boundary with vacuum, whose dispersion crosses the direct band gap at the $(\pi, 0)$ or $(0, \pi)$ -point respectively, while the phase with $C_1 = 2$ (Phase II) has both at its boundary with vacuum.

The chiral magnonic edge modes can be easily twisted or split by the change of the size (λ) and shape (r) of the unit cell, which we demonstrate in Fig. 5a,b. In Fig. 5a, the MC in the phase II ($r = 1$) is connected with the other MC in the phase III ($r > 1$), whose Chern integer for the lowest band differ by unity. The boundary between these two MC systems supports the chiral

magnonic edge mode which runs across the direct band gap at $(0, \pi)$ point. The existence of such an edge mode can be shown from the other 2 by 2 Dirac Hamiltonian derived near $\lambda = \lambda_{c,2}$. This means that the two chiral magnonic edge modes propagating along the boundary of the MC in the phase II ($r = 1$) are spatially divided into two, where one mode goes along the boundary of another MC in the phase III ($r > 1$), while the other goes along the boundary between these two MCs. This configuration realizes a 'spin-wave current splitter', an alternative to those proposed in other geometries.⁴⁰

Discussion

By calculating a newly-introduced bosonic Chern integer for spin wave bands, we argue that two-dimensional normally-magnetized magnonic crystal acquires chiral edge modes for magnetostatic wave in the dipolar regime. Each mode is localized at the boundary of the system, carrying magnetic energies in a unidirectional way. Thanks to the topological protection, spin-wave propagations along these chiral edge modes are generally robust against imperfections of the lattice periodicity and boundary roughness; they are free from any types of elastic backward scatterings with moderate strength.³⁹ This robustness makes it possible a magnonic analogue of Fabry-Perot interferometer as discussed below.

The interferometer is made up of a coupled of chiral magnonic edge modes encompassing a single topological MC (see Fig. 5c). Parts of the MC are spatially constricted by the hole inside, so as to play a role of the 'point contact' between these edge modes.⁴¹ A unidirectional spin-wave propagation is induced in a chiral mode via an antenna attached to the boundary. The wave is divided into two chiral edge modes at a point contact. Two chiral propagations merge into a single chiral propagation at the other point contact. Depending on a phase difference between these two, the superposed wave exhibits either a destructive interference or a constructive one, which is detected as an electric signal from the other antenna. Note that a local application of magnetic field changes the velocity of either one of the two chiral edge modes locally as $v_k = b \rightarrow v_k = b + \Delta b(\mathbf{r})$. This modification results in a phase shift of the wave, which thus changes the interference pattern observed in the output signal. With the use of this local magnetic field as an external control,^{19,42} the interferometer can serve as a solid-state based magnonic logic gate.

Though chiral edge modes are robust against static perturbations, magnetic energies excited in the edge mode decay into either phonon states or other magnon states in the bulk via inelastic scatterings. The associated decay time or coherence length depends on specific materials, and spin wave propagation along the chiral edge mode survives only within this coherence length. Due to the absence of conduction electrons, however, spin waves in magnetic insulators are generally known to have long coherence lengths. For example, the coherence length in YIG in the magnetostatic regime becomes on the order of

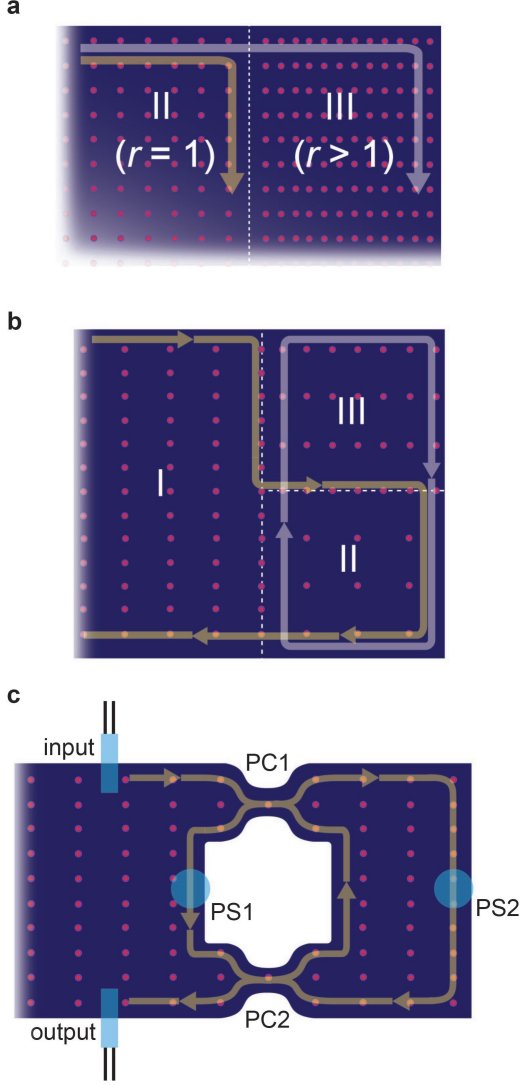


FIG. 5: **Examples of magnonic circuit made by chiral magnonic edge modes.** **a**, Schematic picture of a ‘spin-current splitter’. Two-fold degenerate chiral magnonic edge modes are spatially separated from each other at the interface region between two MCs with different shapes of the unit cell; one with a square unit cell ($r = 1$), while the other with a rectangular unit cell ($r > 1$). **b**, Combination of several MCs with different sizes and shapes of the unit cell channelizes chiral magnonic edge modes at our disposal. Three MCs are used, whose material parameters are taken as those of the phases I, II and III. **c**, Magnonic analogue of the Fabry-Perot interferometer. An electric current in an input antenna induces a chiral magnetostatic wave in the edge mode (yellow arrows). The input wave is split into two at the point contact (PC1). After travelling along different trajectories, these two waves make an interference at the other point contact (PC2). The output wave is measured as an electric signal via the other antenna (output). The phase of the chiral magnetostatic wave in the respective trajectory can be controlled by the local magnetic field applied near the edge modes (PS1 and PS2).

centimeter.²⁰ Thus, all the characteristic spin-wave propagations depicted in Fig. 5a,b,c are experimentally realizable especially in sizable MC systems made out of these magnetic insulators. Measuring these propagations in the space- and time-resolved manner is also experimentally possible in terms of Brillouin light scatterings,⁴³ which is by itself remarkable and which surely leads to the development of innovative spintronic device in future.

Methods

Derivation of equation (10) and material parameters

To introduce the Chern integer for the magnonic bands, we reduced the Landau-Lifshitz equation (7) into an equivalent generalized eigenvalue problem with bosonic quadratic Hamiltonian as in equation (10). To do this, notice first that the commutator between the transverse moments depends on the spatial coordinate, i.e. $[\hat{m}_x(\mathbf{r}), \hat{m}_y(\mathbf{r}')] = M_s(\mathbf{r})\delta(\mathbf{r} - \mathbf{r}')$. To remove this spatial dependence, we normalize the fields as;

$$\beta(\mathbf{r}) \equiv \frac{m_+(\mathbf{r})}{\sqrt{2M_s(\mathbf{r})}}, \quad \beta^\dagger(\mathbf{r}) \equiv \frac{m_-(\mathbf{r})}{\sqrt{2M_s(\mathbf{r})}}. \quad (14)$$

which leads to a proper commutator of the Holstein-Primakoff (HP) boson; $[\hat{\beta}(\mathbf{r}), \hat{\beta}^\dagger(\mathbf{r}')] = \delta(\mathbf{r} - \mathbf{r}')$. In terms of the HP boson fields, the Landau-Lifshitz equation is also properly symmetrized as,

$$\frac{d\beta}{dt} = 4i\alpha(\nabla \cdot Q\nabla)\alpha\beta - 4i\beta(\nabla \cdot Q\nabla)\alpha^2 - iH_0\beta - i\alpha\partial_+\Psi, \quad (15)$$

$$\Delta\Psi = \partial_+(\alpha\beta^\dagger) + \partial_-(\alpha\beta), \quad \partial_\pm \equiv \partial_x \pm i\partial_y, \quad (16)$$

with $\alpha(\mathbf{r}) \equiv \sqrt{M_s(\mathbf{r})/2}$ and $|\gamma|\mu_0$ being omitted for clarity. The static magnetization and exchange interaction are spatially modulated with a lattice periodicity; $\alpha(\mathbf{r}) = \sum_{\mathbf{G}} \alpha(\mathbf{G}) e^{i\mathbf{G}\cdot\mathbf{r}}$ and $Q(\mathbf{r}) = \sum_{\mathbf{G}} Q(\mathbf{G}) e^{i\mathbf{G}\cdot\mathbf{r}}$ with the reciprocal vectors \mathbf{G} . Thus, it follows from the Bloch theorem that $\mathbf{m}(\mathbf{r})$ and $\Psi(\mathbf{r})$ take a form;

$$\beta(\mathbf{r}) = \sum_{\mathbf{k}} \sum_{\mathbf{G}} \beta_{\mathbf{k}}(\mathbf{G}) e^{-i(\mathbf{k}+\mathbf{G})\cdot\mathbf{r}},$$

$$\Psi(\mathbf{r}) = \sum_{\mathbf{k}} \sum_{\mathbf{G}} \Psi_{\mathbf{k}}(\mathbf{G}) e^{-i(\mathbf{k}+\mathbf{G})\cdot\mathbf{r}},$$

where the \mathbf{k} -summation is taken over the first Brillouin zone. In terms of these Fourier modes, an equivalent generalized eigenvalue problem with a quadratic Hamiltonian for the HP field is derived as

$$i\frac{d}{dt} \begin{bmatrix} \beta_{\mathbf{k}} \\ \beta_{-\mathbf{k}}^\dagger \end{bmatrix} = \begin{bmatrix} \beta_{\mathbf{k}} \\ \beta_{-\mathbf{k}}^\dagger \end{bmatrix}, \hat{\mathcal{H}} = \sigma_3 \mathbf{H}_{\mathbf{k}} \begin{bmatrix} \beta_{\mathbf{k}} \\ \beta_{-\mathbf{k}}^\dagger \end{bmatrix}, \quad (17)$$

$$\hat{\mathcal{H}} = \frac{1}{2} \sum_{\mathbf{k}} \begin{bmatrix} \beta_{\mathbf{k}}^\dagger & \beta_{-\mathbf{k}} \end{bmatrix} \mathbf{H}_{\mathbf{k}} \begin{bmatrix} \beta_{\mathbf{k}} \\ \beta_{-\mathbf{k}}^\dagger \end{bmatrix},$$

$$\beta_{\mathbf{k}}^\dagger \equiv [\cdots, \beta_{\mathbf{k}}^\dagger(\mathbf{G}), \cdots, \beta_{\mathbf{k}}^\dagger(-\mathbf{G}), \cdots],$$

$$\beta_{-\mathbf{k}} \equiv [\cdots, \beta_{-\mathbf{k}}(-\mathbf{G}), \cdots, \beta_{-\mathbf{k}}(\mathbf{G}), \cdots].$$

σ_3 in the right hand side takes ± 1 in the particle/hole space, which comes from the commutation relation of bosons, $[\beta_{\mathbf{k}}, \beta_{\mathbf{k}}^\dagger] = 1$ and $[\beta_{\mathbf{k}}^\dagger, \beta_{\mathbf{k}}] = -1$. The comparison between equations (15,16) and equation (17) dictates that $\mathbf{H}_{\mathbf{k}}$ thus introduced is given by a following Hermitian matrix ($\mathbf{H}_{\mathbf{k}}^\dagger = \mathbf{H}_{\mathbf{k}}$);

$$\mathbf{H}_{\mathbf{k}} \equiv \begin{bmatrix} \alpha \cdot \alpha + B_{\mathbf{k}} + H_0 \mathbf{1} & \alpha \cdot \mathbf{I}_{\mathbf{k}} \cdot \alpha \\ \alpha \cdot \mathbf{I}_{\mathbf{k}}^* \cdot \alpha & \alpha \cdot \alpha + B_{\mathbf{k}} + H_0 \mathbf{1} \end{bmatrix} \quad (18)$$

	iron	cobalt	YIG
M_s [$\mu\text{A/m}$]	1.711	1.401	0.140
\sqrt{Q} [\AA]	21.24	28.90	183.57

TABLE I: Saturated magnetization M_s and exchange interaction length \sqrt{Q} of iron, cobalt and yttrium iron garnet (YIG).

with

$$\begin{aligned}
[\alpha]_{\mathbf{G},\mathbf{G}'} &\equiv \alpha(\mathbf{G} - \mathbf{G}'), \quad [\mathbf{I}_{\mathbf{k}}]_{\mathbf{G},\mathbf{G}'} \equiv \delta_{\mathbf{G},\mathbf{G}'} e^{-2i\theta_{\mathbf{k}}(\mathbf{G})}, \\
[\mathbf{B}_{\mathbf{k}}]_{\mathbf{G},\mathbf{G}'} &\equiv 4 \sum_{\mathbf{G}_1, \mathbf{G}_2} \alpha(\mathbf{G} - \mathbf{G}_1) Q(\mathbf{G}_1 - \mathbf{G}_2) \alpha(\mathbf{G}_2 - \mathbf{G}') \\
&\quad \times (\mathbf{k} + \mathbf{G}_1) \cdot (\mathbf{k} + \mathbf{G}_2) \\
&\quad - 4 \sum_{\mathbf{G}_1, \mathbf{G}_2} Q(\mathbf{G}_1) \alpha(\mathbf{G}_2) \alpha(\mathbf{G} - \mathbf{G}' - \mathbf{G}_1 - \mathbf{G}_2) \\
&\quad \times (\mathbf{G} - \mathbf{G}') \cdot (\mathbf{G} - \mathbf{G}' - \mathbf{G}_1), \quad (19)
\end{aligned}$$

and

$$e^{i\theta_{\mathbf{k}}(\mathbf{G})} \equiv \frac{(\mathbf{k} + \mathbf{G})_x + i(\mathbf{k} + \mathbf{G})_y}{|\mathbf{k} + \mathbf{G}|}. \quad (20)$$

After taking the summation over \mathbf{G}_1 and \mathbf{G}_2 in equation (19), one can further decompose $[\mathbf{B}_{\mathbf{k}}]_{\mathbf{G},\mathbf{G}'}$ into three parts,

$$\begin{aligned}
[\mathbf{B}_{\mathbf{k}}]_{\mathbf{G},\mathbf{G}'} &= 4 \sum_{\mu=x,y} [Q\alpha^2]_{\mathbf{G}-\mathbf{G}'} (\mathbf{k} + \mathbf{G})_{\mu} (\mathbf{k} + \mathbf{G}')_{\mu} \\
&\quad + 4i \sum_{\mu=x,y} [Q\alpha(\partial_{\mu}\alpha)]_{\mathbf{G}-\mathbf{G}'} (\mathbf{G} - \mathbf{G}')_{\mu} \\
&\quad + 4 \sum_{\mu=x,y} [Q(\partial_{\mu}\alpha)(\partial_{\mu}\alpha)]_{\mathbf{G}-\mathbf{G}'} \quad (21)
\end{aligned}$$

with

$$\begin{aligned}
[Q\alpha^2]_{\mathbf{G}} &\equiv \frac{1}{S} \int Q(\mathbf{r}) \alpha^2(\mathbf{r}) e^{-i\mathbf{G}\cdot\mathbf{r}} d^2\mathbf{r}, \\
[Q\alpha(\partial_{\mu}\alpha)]_{\mathbf{G}} &\equiv \frac{1}{S} \int Q(\mathbf{r}) \alpha(\mathbf{r}) (\partial_{\mu}\alpha(\mathbf{r})) e^{-i\mathbf{G}\cdot\mathbf{r}} d^2\mathbf{r}, \\
[Q(\partial_{\mu}\alpha)(\partial_{\mu}\alpha)]_{\mathbf{G}} &\equiv \frac{1}{S} \int Q(\mathbf{r}) (\partial_{\mu}\alpha(\mathbf{r})) (\partial_{\mu}\alpha(\mathbf{r})) e^{-i\mathbf{G}\cdot\mathbf{r}} d^2\mathbf{r},
\end{aligned}$$

where the 2- d integrals in the right hand side are taken over the unit cell and S denotes the area of the cell.

Notice that, owing to complex-valued phase factors in the anomalous part, $\mathbf{I}_{\mathbf{k}} \neq \mathbf{I}_{\mathbf{k}}^*$, both the time-reversal symmetry and the mirror symmetries within the 2- d plane are absent in equation (18). Without periodic modulations, $\alpha = \alpha\mathbf{1}$ and $\mathbf{Q} = \mathbf{Q}\mathbf{1}$, these phase factors can be erased by a proper gauge transformation, $\beta_{\mathbf{k}}^{\dagger} \rightarrow \beta_{\mathbf{k}}^{\dagger} \sqrt{\mathbf{I}_{\mathbf{k}}^*}$ and $\beta_{-\mathbf{k}} \rightarrow \beta_{-\mathbf{k}} \sqrt{\mathbf{I}_{\mathbf{k}}}$, so that both symmetries are recovered. In the presence of the periodic modulations, $\alpha \neq \alpha\mathbf{1}$ and $\mathbf{Q} \neq \mathbf{Q}\mathbf{1}$, however, this is not the case and these two symmetries are generally gone.

The specific MC system considered in this paper is composed of two kinds of ferromagnets;^{26,27,32} the respective (square root of) magnetization and (square of) exchange interaction length are specified by (α_j, Q_j) ($j = 1, 2$). The unit cell of the MC is square shaped, inside which one of these two ferromagnets (α_1, Q_1) are embedded within a circular region, while the remaining region is filled with the other (α_2, Q_2). If $\alpha(\mathbf{r})$ has a discontinuity at the boundary between these two regions, the last term in equation (21), $[Q(\partial_{\mu}\alpha)(\partial_{\mu}\alpha)]$, generally diverges, since having the second derivative with respect to a spatial coordinate. Physically, such infrared divergences are removed by a smooth variation of the magnetization at the boundary. For simplicity, we interpolate $\alpha(\mathbf{r})$ as a linear function of the radial coordinate measured from the center of the circular region;

$$\alpha(\mathbf{r}) = \begin{cases} \alpha_1 & (|\mathbf{r}| < R_0) \\ \alpha_1 - \frac{|\mathbf{r}| - R_0}{R_1 - R_0} (\alpha_1 - \alpha_2) & (R_0 < |\mathbf{r}| < R_1) \\ \alpha_2 & (R_1 < |\mathbf{r}|) \end{cases} \quad (22)$$

A discontinuity in $Q(\mathbf{r})$ is also removed by the same linear interpolation. The results in Fig. 2 were obtained from the numerics with $(r_0, r_1) \equiv (R_0/\lambda, R_1/\lambda) = (0.10, 0.125)$, while $(M_{s,0}, M_{s,1}) = (1.752, 0.194)$ [$\mu\text{A/m}$] and $(\sqrt{Q_0}, \sqrt{Q_1}) = (33, 130)$ [\AA].²⁷ As for the material parameters of iron (Fe), cobalt (Co), and YIG, we used the values from the literature³² (Table I). To obtain the para-unitary matrix $\mathbf{T}_{\mathbf{k}}$ which diagonalizes $\mathbf{H}_{\mathbf{k}}$, we employed the method based on the Cholesky decomposition.²⁸

- ¹ Kane, C. L. & Mele, E. J., Quantum Spin Hall Effect in Graphene, *Phys. Rev. Lett.* **95**, 226801 (2005).
- ² Kane, C. L. & Mele, E. J., Z_2 Topological Order and the Quantum Spin Hall Effect, *Phys. Rev. Lett.* **95**, 146802 (2005).
- ³ Bernevig, B. A. & Zhang, S. C., Quantum Spin Hall Effect, *Phys. Rev. Lett.* **96**, 106802 (2006).
- ⁴ Bernevig, B. A., Hughes, T. L. & Zhang, S. C., Quantum Spin Hall Effect and Topological Phase Transition in HgTe Quantum Wells, *Science* **314**, 1757 (2006).
- ⁵ Fu, L., Kane, C. L., & Mele, E. J., Topological insulator in three dimensions, *Phys. Rev. Lett.* **98**, 106803 (2007).
- ⁶ König, M., Wiedmann, S., Brune, C. Roth, A., Buhmann, H., Molenkamp, L. W., Qi, X. L. & Zhang, S. C., Quantum spin Hall insulator state in HgTe quantum wells, *Science*

318, 766 (2007).

- ⁷ Hsieh, D., Qian, D., Wray, L., Xia, Y., Hor, Y. S., Cava, R. J. & Hasan, M. Z., A topological Dirac insulator in a quantum spin Hall phase, *Nature* **452** 970 (2008).
- ⁸ Qi, X. L., Hughes, T. L., & Zhang, S. C., Topological field theory of time-reversal invariant insulators *Phys. Rev. B* **78**, 195424 (2008).
- ⁹ Read, N. & Green, D., Paired states of fermions in two dimensions with breaking of parity and time-reversal symmetries and the fractional quantum Hall effect, *Phys. Rev. B* **61** 10267 (2000).
- ¹⁰ Ivanov, D. A. Non-abelian statistics of half-quantum vortices in p -wave superconductors, *Phys. Rev. Lett.*, **86**, 268 (2001).
- ¹¹ Jang, J., Ferguson, D. G., Vakaryuk, V., Budakian, R.,

- Chung, S. B., Goldbart, P. M. & Maeno, Y., Observation of Half-Height Magnetization Steps in Sr_2RuO_4 , *Science*, **331**, 6014 (2011).
- ¹² Aoki, Y., Wada, Y., Saitoh, M., Nomura, R., Okuda, Y., Nagato, Y., Yamamoto, M., Higashitani, S., & Nagai, K., Observation of surface Andreev bound states of superfluid He-3 by transverse acoustic impedance measurements, *Phys. Rev. Lett.* **95**, 075301 (2005).
- ¹³ Kitaev, A. Y., Unpaired Majorana fermions in quantum wires, *Physics-Uspekhi* **44**, 131 (2001).
- ¹⁴ Haldane, F. D. M. & Raghu, S., Possible Realization of Directional Optical Waveguides in Photonic Crystals with Broken Time Reversal Symmetry, *Phys. Rev. Lett.* **100**, 013904 (2008).
- ¹⁵ Raghu, S. & Haldane, F. D. M., Analogs of quantum-Hall-effect edge states in photonic crystals, *Phys. Rev. A* **78**, 033834 (2008).
- ¹⁶ Wang, Z., Chong, Y., Joannopoulos, J. D., Soljačić, M., Observation of unidirectional backscattering-immune topological electromagnetic states, *Nature* **461**, 772-775 (2009).
- ¹⁷ Damon, R. W., & Eschbach J. R., Magnetostatic modes of a ferromagnet slab, *J. Phys. Chem. Solids* **19** 308 (1961).
- ¹⁸ Damon, R. W., & Van De Vaart, H., Propagation of Magnetostatic spin waves at Microwaves Frequencies in a normally-magnetized disk, *Journal of Applied Physics*, **36**, 3453 (1965).
- ¹⁹ Kryuglyak, V. V., Demokritov, S. O. & Grundler, D. Magnonics, *Journal of Physics D*, **43**, 264001 (2010).
- ²⁰ Serga, A. A., Chumak, A. V. & Hillebrands, B. YIG Magnonics, *Journal of Physics D*, **43**, 264002 (2010).
- ²¹ Lenk, B., Ulrichs, H., Garbs, F. & Münzenberg, M., The building blocks of magnonics, *Physics Reports* **507**, 107-136 (2011).
- ²² Katsura, H., Nagaosa, N. & Lee, P. A., Theory of the Thermal Hall Effect in Quantum Magnets, *Phys. Rev. Lett.* **104**, 066403 (2010).
- ²³ Onose, Y., Ideue, T., Katsura, H., Shiomi, Y., Nagaosa, N. & Tokura, Y., Observation of the Magnon Hall Effect, *Science* **329**, 297 (2010).
- ²⁴ Matsumoto, R., & Murakami, S., Theoretical prediction of rotating magnon wavepacket in ferromagnets, *Phys. Rev. Lett.* **106**, 197202 (2011).
- ²⁵ Matsumoto, R., & Murakami, S., Rotational motion of magnons and the thermal Hall effect, *Phys. Rev. B* **84**, 184406 (2011).
- ²⁶ Vasseur, J. O., Dobrzynski, L., Djafari-Rouhani, B. & Puzskarski, H., Magnon band structure of periodic composites, *Phys. Rev. B* **54**, 1043 (1996).
- ²⁷ Krawczyk, M. & Puzskarski, H., Plane-wave theory of three-dimensional magnonic crystals, *Phys. Rev. B* **77**, 054437 (2008).
- ²⁸ Colpa, J. H. P., Diagonalization of the quadratic boson hamiltonian, *Physica A* **93** (3-4), 327-353 (1978).
- ²⁹ Thouless, D. J., Kohmoto, M., Nightingale, M. P. & den Nijs, M., Quantized Hall Conductance in a Two-Dimensional Periodic Potential, *Phys. Rev. Lett.* **49**, 405 (1982).
- ³⁰ Zhang, C., & Niu, Q., Geometric optics of Bloch waves in a chiral and dissipative medium, *Phys. Rev. A* **81**, 053803 (2010).
- ³¹ Kalinikos, B. A., & Slavin, A. N., Theory of dipole-exchange spin wave spectrum for ferromagnetic films with mixed exchange boundary conditions, *J. Phys. C: Solid State Phys.* **19**, 7013 (1986).
- ³² Sietsema, G., & Flatté, M. E., Magnonic band structure of a two-dimensional magnetic superlattice, [arXiv:1111.2506v1](https://arxiv.org/abs/1111.2506v1).
- ³³ Karplus, M., & Luttinger, J. M., Hall Effect in Ferromagnetics, *Phys. Rev.* **95**, 1154 (1954).
- ³⁴ Onoda, M. & Nagaosa, N., Topological Nature of Anomalous Hall Effect in Ferromagnets, *J. Phys. Soc. Jpn.* **71** 19 (2002).
- ³⁵ Berry, M. V., Quantal Phase Factors Accompanying Adiabatic Changes, *Proc. R. Soc. A* **392**, 45-57 (1984).
- ³⁶ Simon, B., Holonomy, the Quantum Adiabatic Theorem, and Berry's phase, *Phys. Rev. Lett.* **51**, 2167, (1983).
- ³⁷ Su, W. P., Schrieffer, J. R., & Heeger, A. J., Solitons in Polyacetylene, *Phys. Rev. Lett.* **42**, 1698 (1979).
- ³⁸ Niemi, A. J., & Semenoff, G. W., Fermion number fractionalization in quantum field theory, *Physics Report*, **135**, 99 (1986).
- ³⁹ Halperin, B. I., Quantum Hall conductance, current-carrying edge states, and the existence of extended states in a two-dimensional disordered potentials *Phys. Rev. B*, **25**, 2185 (1982).
- ⁴⁰ Demidov, V. E., Jersch, J., Rott, K., Krzysteczko, P., Reiss, G. & Demokritov, S. O., Nonlinear Propagation of Spin Waves in Microscopic Magnetic Stripes, *Phys. Rev. Lett.* **102**, 177207 (2009).
- ⁴¹ Ji, Y., Chung, Y., Sprinzak, D., Heiblum, M., Mahalu, D., & Shtrikman, H., An electronic Mach-Zehnder interferometer, *Nature*, **422**, 415 (2003).
- ⁴² Schneider, T., Serga, A. A., Leven, B., Hillebrands, B., Stamp, R. L., Kostylev, M. P., Realization of spin-wave logic gates, *Applied Physics Letters*, **92**, 022505 (2008).
- ⁴³ Bauer, M., Buttner, O., Demokritov, S. O., Hillebrands, B., Grimalsky, V., Rapoport, Y., & Slavin, A. N., Observation of spatiotemporal self-focusing of spin waves in magnetic films, *Phys. Rev. Lett.* **81**, 3769 (1998).

Acknowledgement

We would like to thank Masayuki Hashisaka for discussions. RS also thanks to Tsutomu Momoi for informing him of Ref. 28. This work is partly supported in part by Grant-in-Aids from the Ministry of Education, Culture, Sports, Science and Technology of Japan (No. 21000004 and 22540327) and by Grant for Basic Scientific Research Projects from the Sumitomo Foundation. We also acknowledge financial support from the Global Center of Excellence Program by MEXT, Japan, through the “Nanoscience and Quantum Physics” Project of the Tokyo Institute of Technology.

Additional Information

The authors declare no competing financial interests.

Author contribution

All authors contributed equally to the manuscript.

Supplementary Information for ‘Topological chiral magnonic edge mode in a magnonic crystal’

Quantization of the Chern number

The Chern number associated with the j -th magnonic band is constructed from the projection operator¹

$$C_j \equiv \frac{i\epsilon_{\mu\nu}}{2\pi} \int_{\text{BZ}} d\mathbf{k} \text{Tr}[(\mathbf{1} - \mathbf{P}_j)(\partial_{k_\mu} \mathbf{P}_j)(\partial_{k_\nu} \mathbf{P}_j)], \quad (\text{S23})$$

where \mathbf{P}_j denotes the projection operator filtering out the j -th band at the momentum \mathbf{k} . The integral is over the first Brillouin zone (BZ) in the two-dimensional \mathbf{k} space. Equation (3) suggests that the projection operator takes a form,

$$\mathbf{P}_j \equiv \mathbf{T}_\mathbf{k} \mathbf{\Gamma}_j \sigma_3 \mathbf{T}_\mathbf{k}^\dagger, \quad (\text{S24})$$

where $\mathbf{\Gamma}_j$ is a diagonal matrix taking +1 for the j -th diagonal component and zero otherwise. With this definition, equation (S24) allows that $\sum_j \mathbf{P}_j = \mathbf{1}$ and $\mathbf{P}_j \mathbf{P}_m = \delta_{jm} \mathbf{P}_j$. C_j defined in equation (S23) reduces to a surface integral of the rotation of the gauge field $A_j \equiv (A_{j,x}, A_{j,y})$ over the BZ, i.e. equations (4-6).

To see its quantization,^{2,3} notice first that such a surface integral reduces to zero, provided that the gauge field is defined uniquely and smoothly over the whole BZ. When any of $[\mathbf{T}_\mathbf{k}]_{a,j}$ has a zero on the BZ, however, the gauge field cannot be determined uniquely over the whole BZ. In this case, we need to decompose the BZ into two overlapped regions³ (H_1 and H_2 with $H_1 \cup H_2 = \text{BZ}$ and $H_1 \cap H_2 = \partial H_1 = -\partial H_2 \equiv \Gamma$), in such a way that one of $[\mathbf{T}_\mathbf{k}]_{a,j}$ (say $[\mathbf{T}_\mathbf{k}]_{1,j}$) does not have any zero within one region (H_1), while another (say $[\mathbf{T}_\mathbf{k}]_{2,j}$) has no zero inside the other (H_2). In the former region, we then take the gauge, $\langle a | \mathbf{u}_{\mathbf{k},j}^{(1)} \rangle \equiv [\mathbf{T}_\mathbf{k}]_{a,j}$, such that $\langle 1 | \mathbf{u}_{\mathbf{k},j}^{(1)} \rangle$ is always real positive, while take another gauge ($|\mathbf{u}_{\mathbf{k},j}^{(2)}\rangle$) in the other (H_2), making $\langle 2 | \mathbf{u}_{\mathbf{k},j}^{(2)} \rangle$ to be always real positive. Provided that the j -th magnonic band considered is isolated from the others ($E_{\mathbf{k},j} \neq E_{\mathbf{k},m \neq j}$ for any \mathbf{k}), these two wavefunctions are always related to each other by a certain $U(1)$ transformation,

$$|\mathbf{u}_{\mathbf{k},j}^{(2)}\rangle = |\mathbf{u}_{\mathbf{k},j}^{(1)}\rangle e^{i\theta_\mathbf{k}}. \quad (\text{S25})$$

Now that the gauge of $|\mathbf{u}_{\mathbf{k},j}^{(a)}\rangle$ and the gauge of $|\mathbf{u}_{\mathbf{k},j}^{(2)}\rangle$ are uniquely defined in H_1 and H_2 respectively, $A_{j,\nu}^{(a)} \equiv i[\sigma_3]_{jj} \langle \mathbf{u}_{\mathbf{k},j}^{(a)} | \sigma_3 \partial_{k_\nu} | \mathbf{u}_{\mathbf{k},j}^{(a)} \rangle$ ($a = 1, 2$) are smooth functions inside each of these two regions. The Stokes theorem is applied separately, so that equation (6) is calculated as,

$$\begin{aligned} C_j &= \frac{1}{2\pi} \int_{H_1} d\mathbf{k} \nabla_\mathbf{k} \times A_j^{(1)} + \frac{1}{2\pi} \int_{H_2} d\mathbf{k} \nabla_\mathbf{k} \times A_j^{(2)} \\ &= \frac{1}{2\pi} \oint_\Gamma d\mathbf{k} \cdot (A_j^{(1)} - A_j^{(2)}) = \frac{1}{2\pi} \oint_\Gamma d\mathbf{k} \cdot \nabla_\mathbf{k} \theta_\mathbf{k}, \end{aligned} \quad (\text{S26})$$

with $\nabla_\mathbf{k} \equiv (\partial_{k_x}, \partial_{k_y})$. Two regions share a boundary (Γ), which forms a closed loop. $\theta_\mathbf{k}$ introduced in equation (S25) generally have a $2\pi n$ phase winding ($n \in \mathbb{Z}$), when \mathbf{k} winds along this loop. Accordingly, the right

hand side is an integer, i.e. $C_j = \mathbb{Z}$. In the actual numerical calculations of C_j , we employed an algorithm based on the ‘manifestly gauge-invariant’ description of the Chern integer.⁴

Magnetic Monopole and Dirac Hamiltonian

When two bosonic (magnonic) bands form a band-touching point in the 3-dimensional \mathbf{p} -parameter space with $\mathbf{p} \equiv (k_x, k_y, \lambda)$, the dual magnetic fields associated with these two bands via equations (5,11,12) generally have a quantized source of their divergence at the point ($\mathbf{p} = \mathbf{p}_c$). To see this, notice first that, away from the band-touching point, $\mathbf{p} \neq \mathbf{p}_c$, the gauge invariant dual magnetic fields for these two bands are uniquely determined, which are therefore divergence-free by their definition. At $\mathbf{p} = \mathbf{p}_c$, however, the projection to each of these two bands cannot be defined, which endows the respective dual magnetic field with some singular structure. To study this structure, one can use the degenerate perturbation theory in a generalized eigenvalue problem. The eigenvalue problem takes a form

$$\mathbf{H}_\mathbf{p} \mathbf{T}_\mathbf{p} = \sigma_3 \mathbf{T}_\mathbf{p} \begin{bmatrix} \mathbf{E}_\mathbf{p} \\ -\mathbf{E}_{\bar{\mathbf{p}}} \end{bmatrix},$$

with $\mathbf{p} \equiv (k_x, k_y, \lambda)$ and $\bar{\mathbf{p}} \equiv (-k_x, -k_y, \lambda)$. The diagonal matrix σ_3 takes +1 for the particle space while takes -1 in the hole space. $\mathbf{E}_\mathbf{p}$ is a diagonal matrix, whose elements give bosonic (magnonic) bands and are physically required to be all positive definite. $\mathbf{H}_\mathbf{p}$ is a Hermitian matrix obtained from a quadratic bosonic Hamiltonian considered. We decompose this into the zero-th order part and the perturbation part;

$$\mathbf{H}_\mathbf{p} = \mathbf{H}_0 + (\mathbf{H}_\mathbf{p} - \mathbf{H}_0) \equiv \mathbf{H}_0 + \mathbf{V}_\mathbf{p}. \quad (\text{S27})$$

with $\mathbf{H}_0 \equiv \mathbf{H}_{\mathbf{p}=\mathbf{p}_c}$. Suppose that \mathbf{H}_0 has two-fold degenerate eigenstates $|\mathbf{u}_j\rangle$ ($j = 1, 2$) with its eigen-frequency $\omega_0 (> 0)$;

$$\mathbf{H}_0 |\mathbf{u}_j\rangle = \sigma_3 |\mathbf{u}_j\rangle \omega_0,$$

where the states are normalized as $\langle \mathbf{u}_j | \sigma_3 | \mathbf{u}_m \rangle = \delta_{jm}$. On introducing the perturbation $\mathbf{V}_\mathbf{p}$, the degeneracy is split into two frequency levels. The eigenstate for the respective eigen-frequency is determined on the zero-th order of $\mathbf{p} - \mathbf{p}_c$ as;

$$\mathbf{T}_\mathbf{p} = \mathbf{T}_0 \mathbf{U}_\mathbf{p} + \mathcal{O}(|\mathbf{p} - \mathbf{p}_c|), \quad (\text{S28})$$

where \mathbf{T}_0 diagonalizes \mathbf{H}_0 with $\mathbf{T}_0^\dagger \sigma_3 \mathbf{T}_0 = \mathbf{T}_0 \sigma_3 \mathbf{T}_0^\dagger = \sigma_3$ and a unitary matrix $\mathbf{U}_\mathbf{p}$ diagonalizes a 2 by 2 Hamiltonian \mathbf{V}_{eff} formed by the two-fold degenerate eigenstates;

$$\mathbf{V}_{\text{eff}} \equiv \begin{bmatrix} \langle \mathbf{u}_1 | \mathbf{V}_\mathbf{p} | \mathbf{u}_1 \rangle & \langle \mathbf{u}_1 | \mathbf{V}_\mathbf{p} | \mathbf{u}_2 \rangle \\ \langle \mathbf{u}_2 | \mathbf{V}_\mathbf{p} | \mathbf{u}_1 \rangle & \langle \mathbf{u}_2 | \mathbf{V}_\mathbf{p} | \mathbf{u}_2 \rangle \end{bmatrix}. \quad (\text{S29})$$

Accordingly, near $\mathbf{p} = \mathbf{p}_c$, the dual magnetic field defined in equations (5,11,12) is given only by this unitary matrix;

$$\mathbf{B}_j = \nabla \times \mathbf{A}_j, \quad \mathbf{A}_j = i \text{Tr}[\mathbf{\Gamma}_j \mathbf{U}_\mathbf{p}^\dagger \nabla \mathbf{U}_\mathbf{p}],$$

with $\nabla \equiv (\partial_{k_x}, \partial_{k_y}, \partial_\lambda)$, while equation (S29) reduces to some 2 by 2 Dirac-type Hamiltonian. From this, we can prove the quantization of the dual magnetic charge at the band-touching point exactly in the same way as in the fermionic systems,^{5,6} where the sign and the strength of the magnetic charge is determined only by the 2 by 2 effective Dirac-type Hamiltonian. With a proper gauge transformation and scale transformation, the effective

Hamiltonians at the band-touching points P_j ($j = 1, 2$) take a form;

$$\mathcal{H}_{\text{eff}} = \omega_0 \tau_0 + (\lambda - \lambda_{c,j}) \tau_3 + ap_x \tau_1 + bp_y \tau_2,$$

with $a > 0$, $b > 0$, $(p_x, p_y) \equiv (k_x - \pi, k_y)$ for $j = 1$ and $(p_x, p_y) \equiv (k_x, k_y - \pi)$ for $j = 2$. From this, equation (13) is derived by the replacement of $p_\mu \rightarrow -i\partial_\mu$.

¹ Avron, J. E., Seiler, R. & Simon, B., Homotopy and Quantization in Condensed Matter Physics, *Phys. Rev. Lett.* **51**, 51 (1983).

² Thouless, D. J., Kohmoto, M., Nightingale, M. P. & den Nijs, M., Quantized Hall Conductance in a Two-Dimensional Periodic Potential, *Phys. Rev. Lett.* **49**, 405 (1982).

³ Kohmoto, M., Topological invariant and the quantization of the Hall conductance, *Ann. Phys. (N.Y.)* **160**, 343, (1985).

⁴ Fukui, T., Hatsugai, Y. & Suzuki, H., Chern Numbers in Discretized Brillouin Zone: Efficient Method of Computing (Spin) Hall Conductances, *J. Phys. Soc. Jpn.* **74**, 1674-1677 (2005).

⁵ Berry, M. V., Quantal Phase Factors Accompanying Adiabatic Changes, *Proc. R. Soc. A* **392**, 45-57 (1984).

⁶ Simon, B., Holonomy, the Quantum Adiabatic Theorem, and Berry's phase, *Phys. Rev. Lett.* **51**, 2167, (1983).